The temporal characteristics of expectations and prediction errors in pain

Andreas Strube[1] , Michael Rose[1] & Christian Büchel[1]

[1]Department of Systems Neuroscience, University Medical Center Hamburg-Eppendorf, 20246 Hamburg, Germany

Corresponding Author: Christian Büchel
Department of Systems Neuroscience
University Medical Center Hamburg-Eppendorf
20246 Hamburg, Germany
Phone: +49 40 7410 57
email: buechel@uke.de

Keywords: pain, expectation, prediction error

In the context of a generative model, such as predictive coding, pain perception can be construed as the integration of expectation and nociceptive input with their difference denoted as a prediction error. In a previous neuroimaging study (Geuter et al., 2017) we observed an important role of the insula in such a model, but could not establish its temporal aspects. Here we employed electroencephalography to investigate neural representations of predictions and prediction errors in heat pain processing. Our data show that alpha-to-beta activity was associated with pain expectation, followed by gamma band activity associated with absolute prediction errors. Source reconstruction revealed the insula as a common region for both effects. This temporal sequence of expectation related alpha-to-beta activity, followed by prediction error associated gamma activity in the insula, provides a possible mechanisms for the temporal integrating of pain predictions and prediction errors in the context of a generative model.

Introduction

It has been shown that physically identical nociceptive input, can lead to variable sensations of pain, depending on contextual factors (Tracey and Mantyh, 2007). In particular, attention, reappraisal and expectation are core mechanisms that influence how nociception leads to pain (Wiech et al., 2008). A clinically important example of how expectations can shape pain processing is placebo hypoalgesia: pain relief mediated by expectation and experience - in the absence of active treatment (Petrovic et al., 2002; Wager et al., 2004; Colloca and Benedetti, 2005; Bingel et al., 2006; Atlas and Wager, 2012; Anchisi and Zanon, 2015).

In the context of a generative model of pain, it has been proposed that pain perception can be seen as the consequence of an integration of expectations with nociception (Büchel et al., 2014; Wiech, 2016; Ongaro and Kaptchuk, 2019). In this framework, expectations are integrated with incoming nociceptive information and both are weighted by their relative precision (Grahl et al., 2018) to form a pain percept. This can be seen in analogy to ideas in multisensory integration (Ernst and Banks, 2002). Expectations or predictions and resulting prediction errors also play a key role in generative models such as predictive coding (Huang and Rao, 2011). In essence, this framework assumes that neuronal

assemblies implement perception and learning by constantly matching incoming sensory data with the top-down predictions of an internal or generative model (Knill and Pouget, 2004; Huang and Rao, 2011; Clark, 2013). Basically, minimizing prediction errors allows systems to resist their tendency to disorder by the creation of models with better predictions regarding the sensory environment, leading to a more efficient encoding of information (Friston, 2010).

Cued pain paradigms (Atlas et al., 2010) have been used to generate expectations and prediction errors. Previous fMRI studies have suggested an important role of the anterior insular cortex for mediating expectation effects and the integration of prior expectation and prediction errors in the context of pain (Ploghaus et al., 1999; Koyama et al., 2005; Atlas et al., 2010; Geuter et al., 2017; Fazeli and Büchel, 2018). These studies have revealed that neuronal signals in the anterior insula represent predictions and prediction errors with respect to pain, which in theory would allow the combination of both terms as required for predictive coding (Büchel et al., 2014; Ongaro and Kaptchuk, 2019). However, in fMRI studies predictions and prediction errors cannot be temporally dissociated due to the low temporal resolution of the method. To investigate this further, we conducted a cue based pain experiment using EEG to achieve high temporal and spectral resolution of predictions and prediction error processes in the context of pain.

In this experiment (n=29) we employed contact heat stimuli with three different intensities (warm, mildly painful, painful), preceded by a visual cue indicating the upcoming intensity (Figure 1). To study modality effects we also presented aversive pictures with 3 levels of aversiveness. To generate prediction errors, the modality (picture or pain) was correctly cued only in 70% of all trials and stimulus intensities were correctly cued only in 60% of all trials. We then investigated oscillatory activity related to stimulus intensity, expectation and prediction errors (Figure 2).

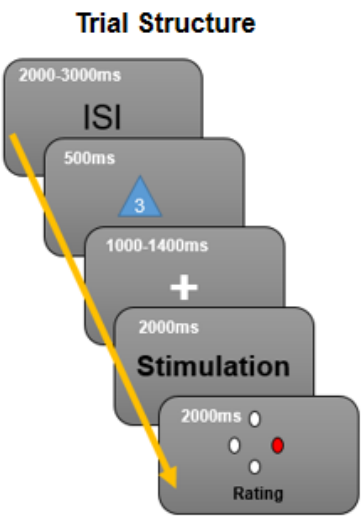

Cue-Stimulus Contingencies

	42°C	46°C	48°C	Picture Level 1	Picture Level 2	Picture Level 3
1	7.0%	2.3%	2.3%	3.0%	1.0%	1.0%
2	2.3%	7.0%	2.3%	1.0%	3.0%	1.0%
3	2.3%	2.3%	7.0%	1.0%	1.0%	3.0%
1	3.0%	1.0%	1.0%	7.0%	2.3%	2.3%
2	1.0%	3.0%	1.0%	2.3%	7.0%	2.3%
3	1.0%	1.0%	3.0%	2.3%	2.3%	7.0%

Figure 1. Left: Graphical representation of the trial structure. Each trial started with the presentation of a cue, indicating the stimulus intensity and modality of the following stimulus. After a jittered phase where only the fixation cross was shown, the stimulus (visual or thermal) was presented. A rating phase (1-4) of the stimulus aversiveness followed. Right: Contingency table for all conditions for each cue-stimulus combination. Note that percentages are for all trials, therefore each row adds up to 1/6 (6 different cues).

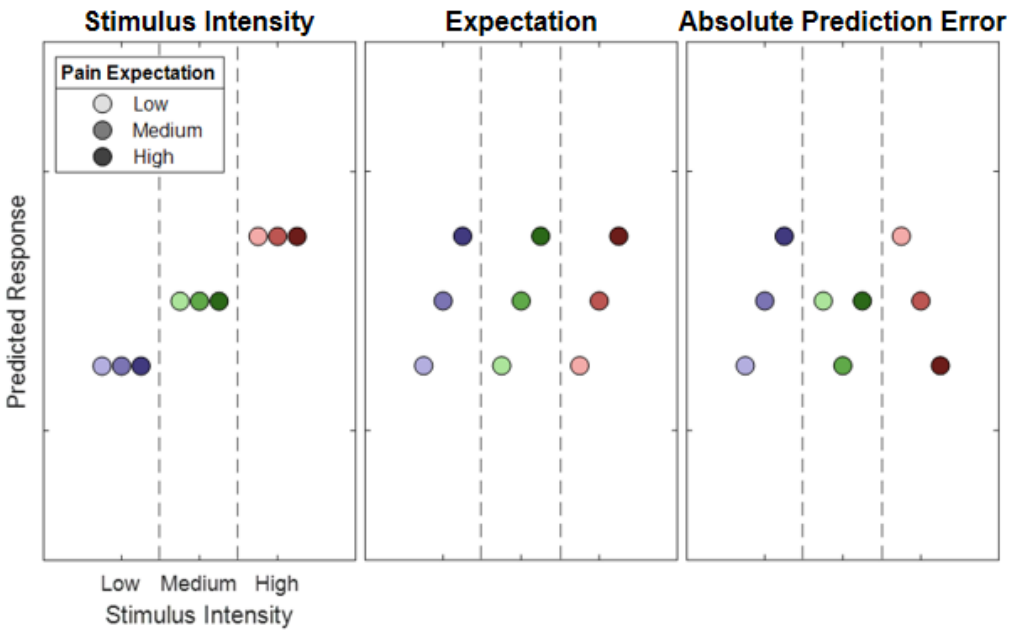

Figure 2. Hypothetical response patterns based on Stimulus Intensity (left), Expectation (middle) and Absolute Prediction Error (right) factors. A combination of all three terms results in a full predictive coding model.

Based on previous data, we (i) hypothesized that expectation signals should temporally precede prediction error signals. (ii) Based on the functional neuroanatomy of cortical microcircuits (Bastos et al., 2012), with feedforward connections predominately

originating from superficial layers and feedback connections from deep layers, we expect that prediction error signals should be related to higher frequencies (e.g. gamma band) than prediction signals (Todorovic et al., 2011; Arnal and Giraud, 2012). Finally, based on our previous fMRI results (Geuter et al., 2017; Fazeli and Büchel, 2018) we expect these effects to include the insular cortex and in particular the anterior insula.

Results

Behavioral data - pain ratings

Participants experienced aversive heat or saw picture stimuli which were probabilistically cued in terms of modality and intensity, evoking an expectation of modality and intensity. The subsequently applied stimuli were then rated on a visual analog scale (VAS) from 1-4. Our primary behavioral question was whether ratings are influenced by the experimental manipulation of stimulus intensity, expectation and absolute prediction errors.

To validate our intensity manipulation for heat pain and to verify the discriminability between different levels of pain, we first tested for the main effect of stimulus intensity (Figure 3a). Our data show a clear rating difference between the three levels of pain. Results regarding the aversive pictures are not the focus of this report but are depicted in Figure 3b for the sake of comparison.

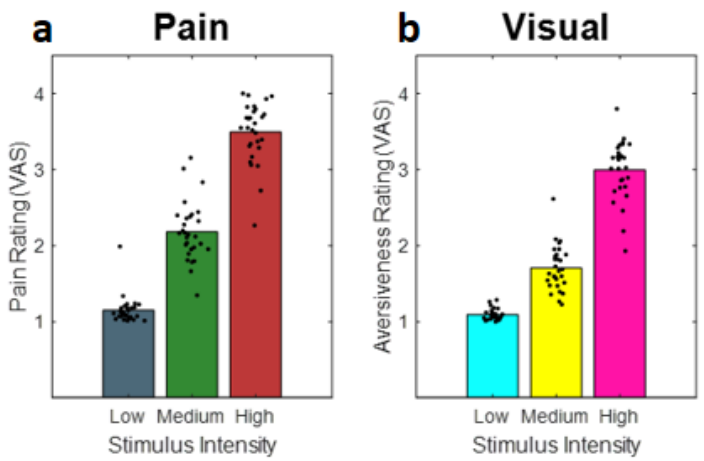

Figure 3. Bars indicate pooled aversiveness ratings for a) pain and b) aversive pictures for low, medium and high intensity conditions. Dots indicate average single subject ratings.

To evaluate the main effects of stimulus intensity, expectation and absolute prediction error, we employed a repeated measures ANOVA of the behavioral data, which revealed significant effects for the main effect of stimulus intensity, i.e. the three levels of pain ($F(2,28) = 743.97$, $p < .001$). Also, the main effect for expectation on pain ratings was significant ($F(2,28) = 38.53$, $p = < .001$) (Table 1), indicating an influence of the cued intensity on behavioral pain ratings. The absolute difference between the cued intensity and the actual stimulus intensity (i. e. prediction error), did not yield a significant effect on pain ratings ($F(2,28) = 2.87$, $p = .10$). The results regarding the aversive pictures are summarized in Table 1.

Factor	Stimulus Intensity (INT)		Cued Intensity (EXP)		Absolute Prediction Error (ERR)	
	F(2,28)	*p*	*F(2,28)*	*p*	*F(2,28)*	*P*
Modality						
Pain	743.97	< .001	39.53	< .001	2.87	.10
Picture	762.10	< .001	1.46	.24	7.7	.01

Table 1. Main effects of stimulus intensity, expectation and absolute prediction errors on subjective ratings in both pain and picture conditions.

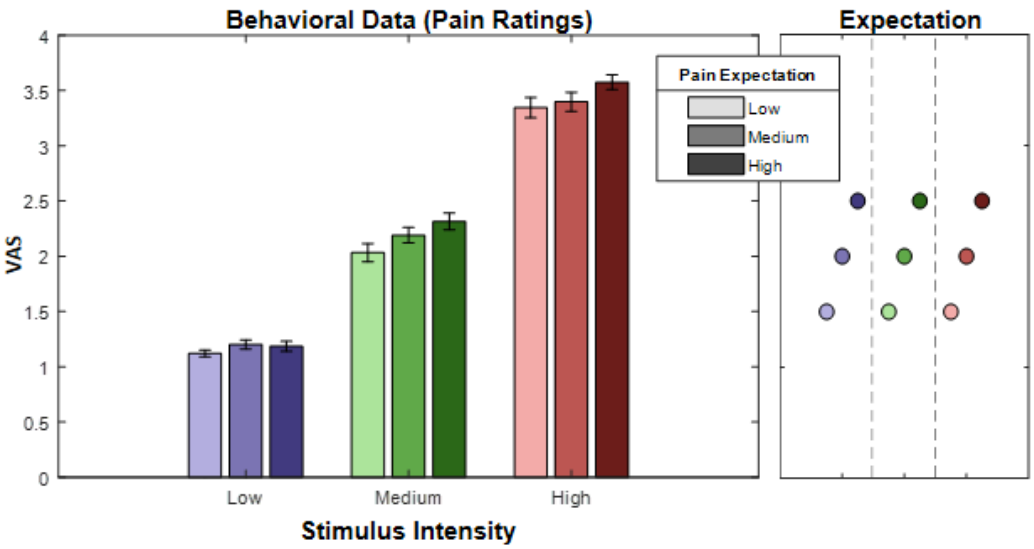

Figure 4. Ratings for painful stimuli (left) and "expectation factor" weights (right). Bars indicate average pain ratings. Ratings were given on a scale from 1 to 4. Error bars depict SEM. The data shows both an effect of stimulus intensity (increase from blue to green to red), but also an effect of expectation (low to medium to high expectation).

EEG - Stimulus Intensity

In a first EEG analysis, we tested for a main effect of the intensity of the nociceptive input in the context of a correctly cued modality (i.e. pain was expected and received). In order to do so, we performed a repeated measures ANOVA on the time-frequency representation of the EEG data on low frequencies (1-30Hz) and high frequencies (31-100Hz) separately after pain onset using a cluster correction criterion to address the multiple comparisons problem (see Methods for details). Any significant cluster – composed of neighboring data points in time, frequency and space – would indicate a neuronal oscillatory representation of variations in stimulus intensity in a given frequency band.

In the low frequency (1-30Hz) range, one positive cluster (i.e. a positive average slope of the factor) and one negative cluster (i.e. a negative average slope of the factor) were significant (Figure 5a), indicating a linear association of stimulus intensity and power in this frequency range. Specifically, the negative cluster included samples in a time range from 250 to 1600ms after pain onset in a frequency range from 5 to 30Hz, predominately at contralateral central electrode sites ($p < .001$). The highest parametric F-value within this cluster obtained from the repeated measures ANOVA was $F(2,28) = 40.87$, ($p < .001$). This sample was found at 1250ms and 13Hz and had a maximum at channel C4.

Also in the low frequency range (1-30Hz), the positive cluster included samples in a time range from 150 to 1250ms after pain onset in a frequency range from 1 to 7Hz at central electrode sites ($p = .038$). The highest parametric F-Value from the repeated measures ANOVA was $F(2,28) = -40.87$, ($p < .001$). This sample was found at 550ms and 1Hz and had a maximum at channel Cz.

In the high frequency range (31-100Hz) representing Gamma activity one positive cluster was significant (Figure 5). This cluster included samples in a time range from 500 to 1600ms after pain onset and frequencies from 37 to 100Hz, predominately at contra-lateral central electrode sites. The highest parametric F-value within this cluster obtained from the repeated measures ANOVA was $F(2,28) = 21.30$, ($p < .001$). This sample was found at 600ms and 60Hz and had a maximum at channel FCz.

In conclusion, these results indicate that a higher intensity of the nociceptive input is associated with increased theta and gamma band power and a negative relationship of alpha-to-beta band power and the intensity of the nociceptive input.

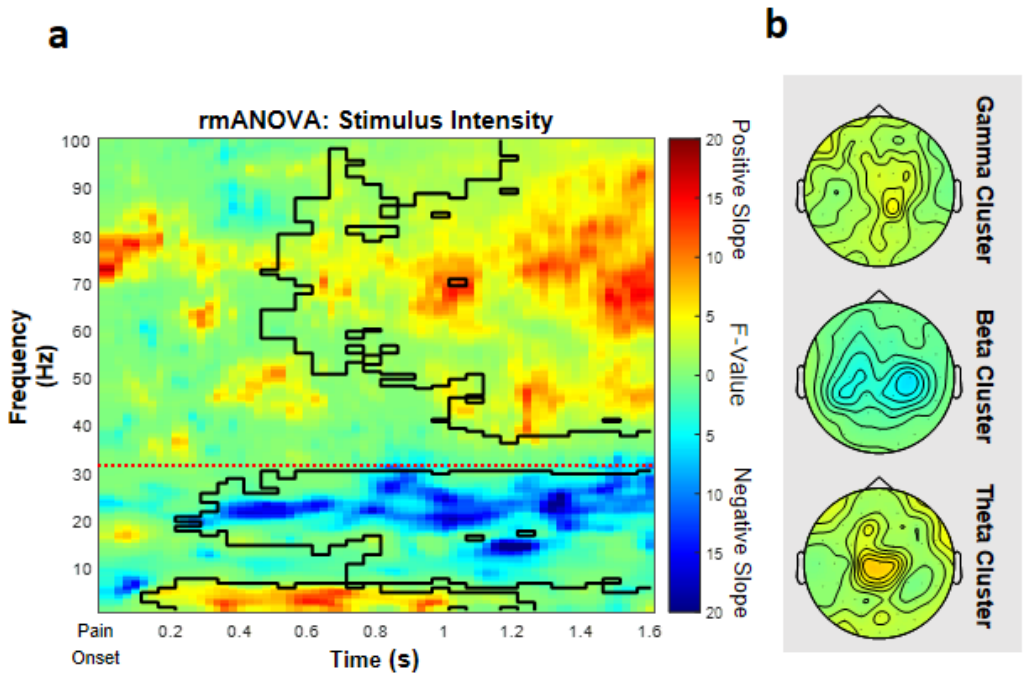

Figure 5. Parametric effects of pain intensity. Time-frequency representation (a) and topographies (b) of the stimulus intensity main effect of the repeated measures ANOVA depicting increases (warm) and decreases (cold) in power in relation to pain stimulus intensity. Data shown for channel C2. Significant clusters are highlighted. Colors represent F-values from the repeated measures ANOVA statistics for the main effect of stimulus intensity.

Expectation

In a next step, we investigated the representation of the expectation factor in our repeated measures model, again for low frequencies (1-30Hz) and high frequencies (31-100Hz) separately in the cue-locked time-frequency representation of the EEG data.

This analysis revealed a significant positive cluster in the low frequency range (1-30Hz), indicating a linear association of cue intensity (EXP) and power in this frequency range ($p = .031$). This expectation cluster included samples from time points ranging from 1200ms to 2050ms after cue onset. The highest parametric statistical test value ($F(2,28) = 27.20$, $p < .001$) was found at channel F2 1700ms after cue onset at a frequency of 15Hz. For source reconstruction using eLORETA (Pascual-Marqui, 2007), a region-of-interest was defined based on the whole time-frequency range of the cluster. Source reconstruction suggests the left and right insular cortices as neuronal generators of the main effect of

expectation (see Figure 6 for a summary of the results; see Supplementary Materials for a full representation of the source reconstruction).

In summary, these results suggest a decrease in alpha-to-beta band power to be associated with our experimental manipulation of expectations regarding the intensity of the nociceptive input. Further, source reconstruction reveals the right insula as a potential neuronal generator of this oscillatory effect.

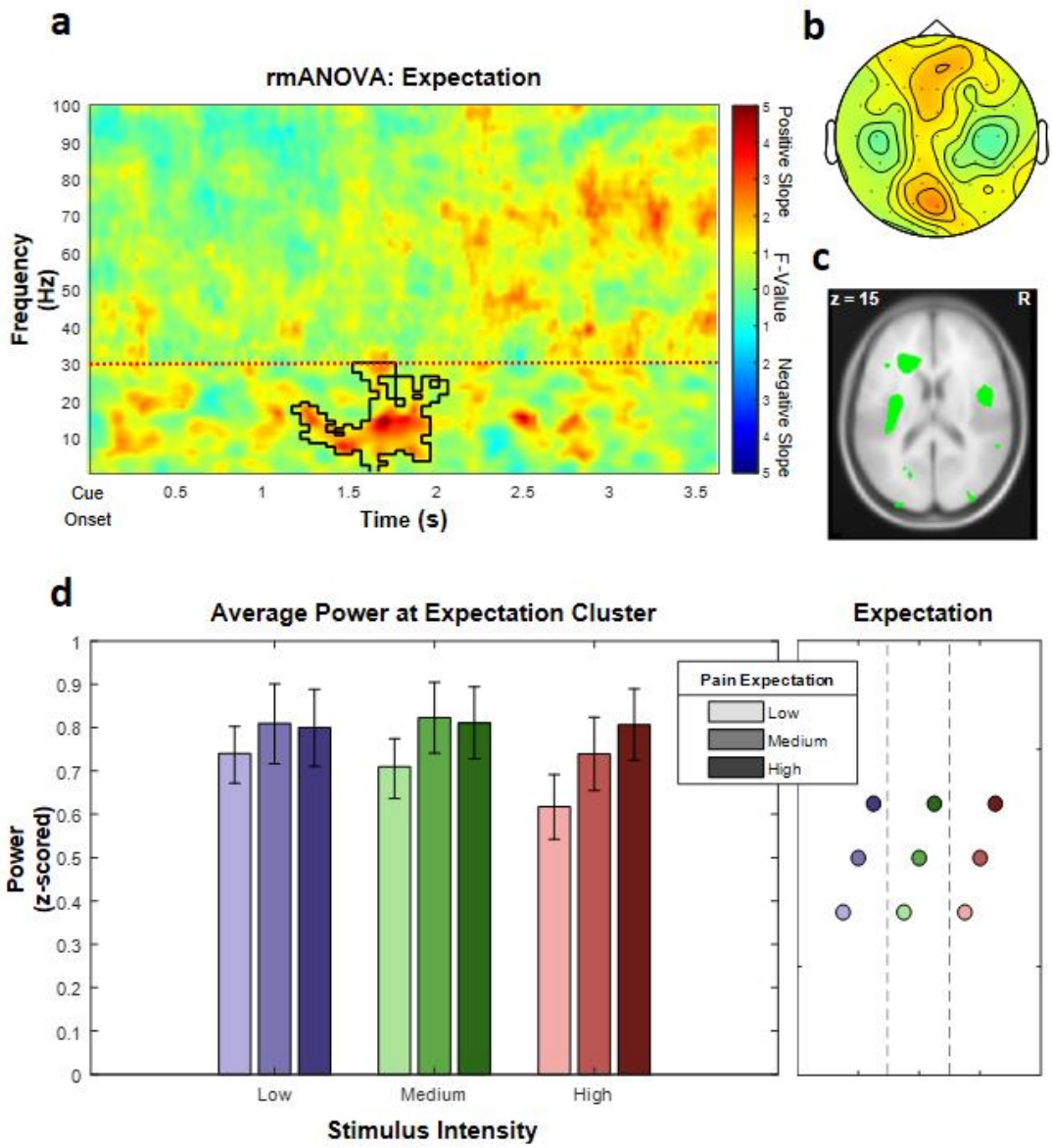

Figure 6. Summary of the main effect of expectation: a) Time-frequency representation of the statistical F-values averaged over significant channels. The significant cluster is highlighted. b) Topography of the averaged power over time and frequency at each channel, brighter colors indicate higher F-values. c) Reconstructed sources, representing the top 2.5% statistical values in source space overlaid on a structural MR template, showing the cluster including the right insular cortex. d) Power values for all conditions with a valid modality cue (expect pain receive pain) averaged over channels and time period of the cluster show alpha-to-beta enhancement (i.e.

positive representation) associated with expectation. Error bars represent SEM. Predicted responses based on the positive expectation factor are shown (right column).

Prediction Error Model

Likewise, clustering was performed for the prediction error term after pain onset in low (1-30Hz) and high frequencies (31-100Hz). Any significant cluster would associate oscillatory activity with the difference of the expectation regarding the intensity of the nociceptive stimulation and the actual stimulation, representing a violation of this expectation (prediction error).

This analysis revealed a significant negative cluster in the high frequency range (31-100Hz), indicating a linear association of absolute prediction errors (ERR) and power in this frequency range ($p = .007$). This absolute prediction error cluster included samples from frequencies ranging from 57 to 100Hz and time points ranging from 250ms to 1400ms after pain onset. The highest parametric statistical test value ($F(2,28) = 24.17$, $p < .001$) was found at channel F3 1200ms after pain onset at a frequency of 87Hz. In the same manner as for the previously reported expectation cluster, source reconstruction using eLORETA (Pascual-Marqui, 2007) was applied with a region-of-interest defined based on the whole time-frequency range of the cluster. Source reconstruction suggests several potential generators of the absolute prediction error effect, including the right insula (see Figure 6 for a summary of the results; see Supplementary Materials for a full representation of the source reconstruction).

In summary, these results suggest a decrease in gamma band power to be associated with our experimental manipulation of expectation violations, resulting from a mismatch of the cued intensity and the actual nociceptive input. Further, source reconstruction reveals the right insula as a potential neuronal generator of this effect.

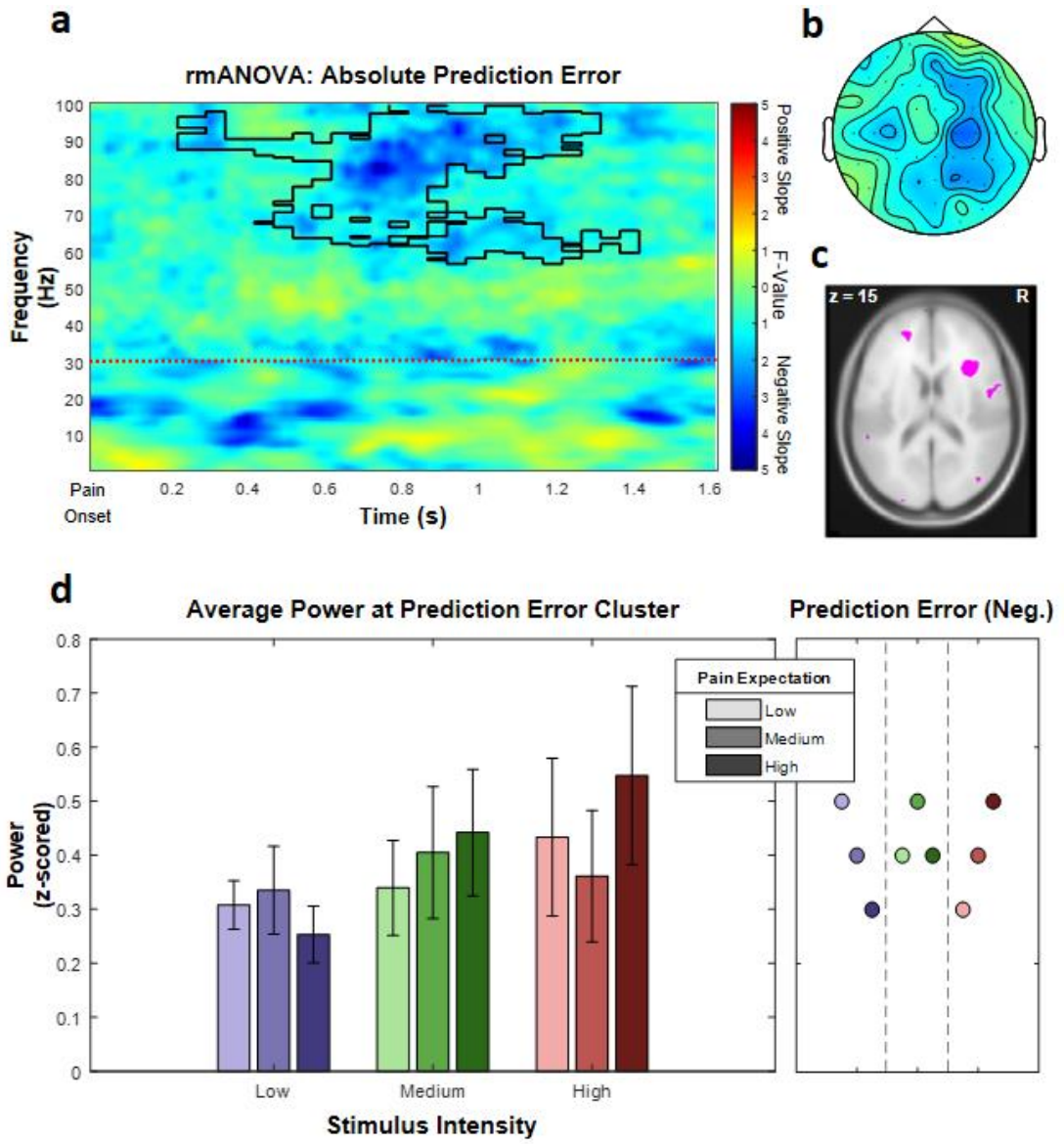

Figure 7. Summary of the main effect of absolute prediction errors: a) Time-frequency representation of the statistical F-values averaged over significant channels. The significant cluster is highlighted. b) Topography of the averaged power over time and frequency at each channel, brighter colors indicate higher F-values. c) Reconstructed sources, representing the top 2.5% statistical values in source space overlaid on a structural MR template, showing the cluster including the right insular cortex. d) Power values for all conditions with a valid modality cue (expect pain receive pain) averaged over channels and time period of the cluster show gamma suppression (i.e. negative representation) associated with expectation. Error bars represent SEM. Predicted responses based on the negative prediction error factor are shown (right column).

Discussion

Summary

Using a cued pain paradigm with three different pain intensities, our data showed a clear discriminability of different levels of pain based on behavioral ratings and EEG time-

227 frequency patterns. Specifically, we observed several clusters of activity to be associated
228 with the intensity of thermal stimulation in the theta, beta and gamma band. Furthermore,
229 behavioral data clearly indicated a positive influence of cued intensity on pain perception.
230 In addition, our results provide evidence for temporally and spectrally separable clusters
231 of oscillatory activity associated with expectation and prediction errors for pain.
232 Specifically, an early (350-600ms) low frequency (1-30Hz) cluster was related to
233 expectation i.e. cued intensity. In contrast, a later occurring cluster at higher frequencies
234 (31-100Hz) was related to prediction errors.

235 Stimulus intensity and oscillatory activity

236 Note that our definition of pain onset is based on the moment the thermode reached the
237 target temperature. Using a thermode heating gradient of 40°C/s and neglecting any small
238 internal delays, the target temperatures of 42, 46 and 48°C are reached after 225, 325 and
239 375ms respectively. Therefore our observed increase in theta power agrees with previous
240 studies (Ploner et al., 2017) and most likely correspond to pain-related evoked potentials
241 (Lorenz and Garcia-Larrea, 2003; Tiemann et al., 2015), such as the P2 with a similar
242 topography (cf. Figure 4b). In addition we observed a significant suppression of alpha-to-
243 beta activity which, given the above mentioned delays of our painful stimuli, is in line with
244 the reported beta suppression in previous EEG studies on pain (Ploner et al., 2006).
245 Finally, power in the gamma band was also correlated with pain intensity, which is in line
246 with previous studies (Zhang et al., 2012).

247 Hypotheses based on microcircuits

248 Theoretical accounts (Arnal and Giraud, 2012; Bastos et al., 2012) have suggested that
249 predictive coding mechanism could be related to the functional architecture of neuronal
250 microcircuits. As feedforward connections are predominately originating from superficial
251 layers and feedback connections from deep layers, it has been suggested that prediction
252 errors should be expressed by higher frequencies than the predictions that accumulate
253 them.

254 In the auditory modality, these ideas are supported by empirical data (Todorovic et al.,
255 2011) showing that prediction errors in the context of repetition suppression were
256 associated with higher gamma band activity. Likewise, in the visual domain, an MEG study
257 has shown that temporo-parietal beta power was correlated with the predictability of an

action kinematics-outcome sequence, while gamma power was correlated with the prediction error (van Pelt et al., 2016).

Frequency Patterns in Predictive Coding of Pain

Our results are fully in line with this hypothesis, namely showing that higher frequencies (gamma band) are related to prediction errors, whereas lower frequencies (alpha-to-beta) were related to expectations. Only a few studies have investigated the spectral and temporal properties of expectations and prediction errors in the context of pain (Ploner et al., 2017). A recent study in rodents has suggested an information flow between S1 gamma and ACC beta activity during spontaneous pain (Xiao et al., 2019). Based on these data, the authors have proposed a predictive coding model including a bottom-up (gamma) and top-down (beta) component (Song et al., 2019). Finally, in humans a recent EEG study showed that the sensorimotor cortex is more strongly connected to the medial prefrontal cortex at alpha frequencies during tonic pain, suggesting alpha band activity in tonic pain to be associated with bottom-up instead of top-down signaling (Nickel et al., 2020). Nevertheless, the focus of these studies was on generic interactions (i.e. top down versus bottom up) processes without directly inducing prediction errors as in a cued pain paradigm employed in our study.

In the flexible routing model proposed by Ploner et al. (2017), pain is seen as driven by contextual processes, such as expectations, which is associated with alpha/beta oscillations and alpha/beta synchrony across brain areas. Previous studies have started to examine the spectral properties of mechanisms related to generative models of pain perception. In particular, a previous MEG study reported that alpha suppression in the anterior insula is related mainly to pain expectation in a paradigm in which painful stimuli were interleaved with non-painful stimuli (Franciotti et al., 2009). This was interpreted as a preparatory mechanism for an upcoming painful stimulus. In a related study, alpha desynchronization in the context of predictable painful stimuli, has been discussed as a possible neural correlate of attentional preparatory processes (Babiloni et al., 2003).

Expectation is also a crucial ingredient of placebo analgesia and nocebo hyperalgesia. A previous study reported that resting state alpha band activity was also linked to the expectation of pain modulation (analgesia) in a placebo paradigm (Huneke et al., 2013). Source localization linked this effect to the insula, the medial frontal and prefrontal cortex.

With respect to negative expectations, it has been shown that pain modulation due to nocebo expectation is associated with enhanced alpha activity (Albu and Meagher, 2016). Our findings are in line with these results indicating an important role of low frequency activity in mediating expectation effects in a pain network underlying a generative model for pain perception.

Insula

Source localization revealed an overlap of potential sources for the expectation related power changes in the alpha-to-beta band and the later prediction error related power changes in the gamma band in the contralateral insular cortex. A previous study (Geuter et al., 2017) used a similar model comparison strategy and identified fMRI activation patterns in the anterior insula to be related to expectation and prediction errors. This was later replicated (Fazeli and Büchel, 2018), again showing that fMRI activity in the anterior insula was best explained by a model combining expectation and prediction errors. Although these studies revealed expectation and prediction error effects in the insula, they were unable to provide deeper mechanistic insights into the temporal orchestration of these effects due to the limited temporal resolution of the hemodynamic response function as measured in fMRI.

Importantly, here we can show that although both effects are co-localized in the insula (Figure 8b), there is a precise temporal and spectral organization of both effects within the insula. Initially, low frequency activity is linked to expectation effects which after integration with nociceptive information can lead to a prediction error expressed by activity in the gamma band. This is further supported by the estimated topographies of the effects. Main effects of stimulus intensity, expectation and absolute prediction errors are all represented by a parietal-to-frontal pattern of activation, suggesting a similar associative network to be at play (see Figure 9 for a schematic summary of the results).

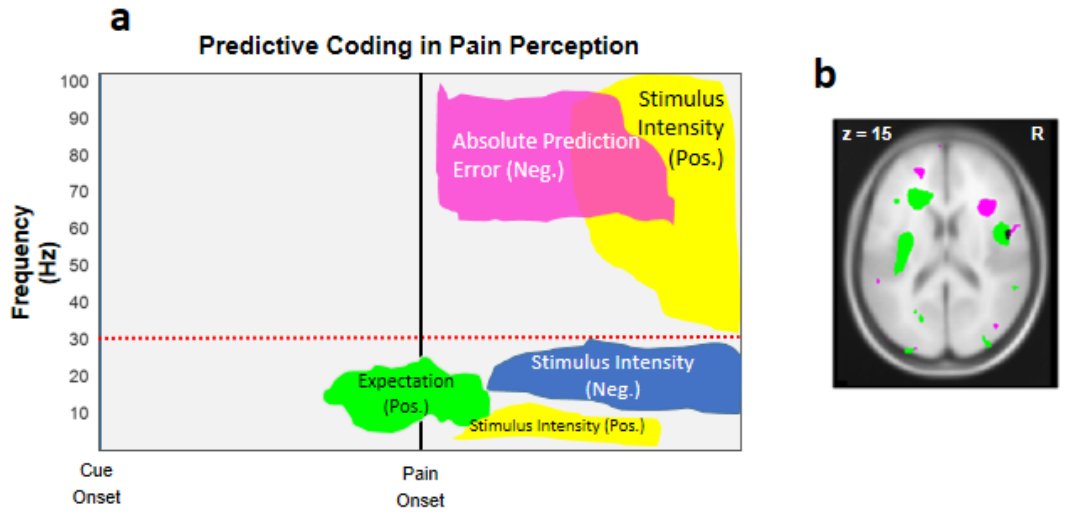

Figure 9. All found clusters of stimulus intensity, expectation and absolute prediction error are displayed in a schematic time-frequency plot (a). The orthographic representation of the source localization of the expectation and prediction error clusters (b): green represents expectation, magenta represents absolute prediction error. Overlay of expectation and absolute prediction error are shown in a darker color.

Limitations

To unravel, the temporal aspects of expectations and prediction errors, this study has been designed in close analogy to a previous fMRI study and we decided to use the same experimental paradigm (Fazeli and Büchel, 2018). We therefore decided to also keep the sample characteristics similar and restricted the sample to male participants, which means that we cannot generalize our results to the population. However, our study agrees with findings of a previous study using a similar design (Geuter et al., 2017) and which tested male and female participants. Future studies should investigate samples including female participants. This would also allow to investigate sex effects with respect to expectation and prediction error effects in pain.

Although EEG has an excellent temporal resolution, its spatial resolution is limited. Consequently, the source reconstruction using LORETA is of low spatial resolution (Pascual-Marqui et al., 1994). However, considering the involvement of the insula in the LORETA source localization together with two previous fMRI studies employing the same (Fazeli and Büchel, 2018) and a very similar design (Geuter et al., 2017) strengthen our confidence that the temporally resolved sources in the alpha-to-beta band for

338 expectations and the later gamma band activity for prediction errors are at last partially
339 originating from the insula.

340 ### Summary

341 Our data show that key variables required for pain perception in the context of a
342 generative model are correlated with distinct oscillatory profiles in the insula.
343 Furthermore, each oscillatory frequency band was correlated with a distinct variable such
344 as expectation and prediction errors. These mechanistic insights could be very helpful in
345 patients with acute and more importantly in patients with chronic pain, where
346 expectations have been shown to play a critical role in pain persistence.

347 ## Methods

348 ### Participants

349 We investigated 35 healthy male participants (mean 26, range: 18–37 years), who were
350 paid as compensation for their participation. Applicants were excluded if one of the
351 following exclusion criteria applied: neurological, psychiatric, dermatological diseases,
352 pain conditions, current medication, or substance abuse. All volunteers gave their
353 informed consent. The study was approved by the Ethics board of the Hamburg Medical
354 Association. Of 35 participants, data from six participants had to be excluded from the
355 final EEG data analysis due to technical issues during the EEG recording (i.e.: the data of
356 the excluded participants were contaminated with excessive muscle and/or technical
357 artifacts) leaving a final sample of 29 participants. The sample size was determined
358 according a power calculation (G*Power V 3.1.9.4) based on (Geuter et al., 2017). For the
359 left anterior insula (fMRI; Table 1 in Geuter et al., 2017) we observed an effect size of
360 partial eta squared of 0.17 and an effect size of 0.22 for the right anterior insula (Cue x
361 stimulus interaction). Using a power of (1-beta) of 0.95 and an alpha level of 0.05 and
362 assuming a low correlation (0.1) between repeated measures, this leads to a sample size
363 of 25 assuming the weaker effect in the left insula.

364 ### Stimuli and Task

365 Thermal stimulation was performed using a 30 × 30 mm^2 Peltier thermode (CHEPS
366 Pathway, Medoc) at three different intensities: warm (42°C), medium painful (46°C), and
367 highly painful (48°C) at the left radial forearm. The baseline temperature was set at 33°C

368 and the rise rate at 40°C/s. After two blocks, the stimulated skin patch was changed to
369 avoid sensitization.

370 As in a previous study (Fazeli and Buechel, 2019) we also used an additional aversive
371 modality, namely aversive pictures. As before, these stimuli were chosen from the
372 International Affective Picture System (IAPS) (Lang, 2005) database at three different
373 levels of aversiveness. The images presented during the EEG experiment had three levels
374 of valence of which the low valence category had valence values of 2.02±0.05 (mean ±
375 standard error), the medium valence category had valence values of 4.06±0.02 (mean ±
376 standard error) and the high valence category had valence values of 5.23±0.01 (mean ±
377 standard error).

378 Prior to each picture or heat stimulus, a visual cue was presented. The color of the cue
379 (triangle) indicated (probabilistically) the modality of the stimulus (orange for picture
380 and blue for heat). A white digit written inside of each triangle indicated
381 (probabilistically) the intensity of the subsequent stimulus (1, 2 and 3 for low, medium
382 and high intensity). During the whole trial, a centered fixation cross was presented on the
383 screen.

384 Each trial began with the presentation of the cue for 500ms as an indicator for the
385 modality and intensity of the subsequently presented stimulus. The modality was
386 correctly cued in 70% of all trials by the color of the triangle. In 60% of all trials, the
387 stimulus intensity was correctly indicated by the digit within the triangle (see Fig. 1b for
388 an overview of all cue contingencies).

389 Before the presentation of the stimulus, there was a blank period with a variable time
390 frame between 1000ms and 1400ms. Then, the visual or thermal stimulus was presented
391 for a duration of two seconds. The visual stimulus was centered on the screen and allowed
392 the participant to perceive the stimulus without eye movements. Right after the
393 termination of the stimulus, subjects were asked to rate the aversiveness of the stimulus
394 on a four point rating scale, where 1 was labeled as "neutral" and 4 was labeled as "very
395 strong". Ratings were performed using a response box operated with the right hand (see
396 Figure 1 for a visualization of the trial structure).

397 In addition, four catch trials were included in each block. Subjects were asked to report
398 the preceding cue in terms of their information content of the modality and intensity
399 within 8s and no stimulation was given in these trials.

400 Trials were presented in four blocks. Each block consisted of 126 trials and four catch
401 trials and lasted about 15 minutes. The trial order within each block was
402 pseudorandomized. The order of blocks was randomized across subjects. The whole EEG
403 experiment including preparation and instructions lasted for about three hours.

404 Prior to the actual EEG experiment, subjects participated in a behavioral training session.
405 During this session, participants were informed about the procedure and gave their
406 written informed consent. The behavioral training session was implemented to avoid
407 learning effects associated with the contingencies between the cues and the stimuli during
408 the EEG session. Between two and three blocks were presented during the training
409 session (without electrophysiological recordings). The experimenter assessed the
410 performance after each block based on the percentage of successful catch trials and the
411 ability to distinguish the three levels of aversiveness of each modality. The training
412 session was terminated after the second block if participants were able to successfully
413 label cues in 75% of the catch trials within the current block.

414 EEG Data Acquisition

415 EEG data were acquired using a 64-channel Ag/AgCl active electrode system (ActiCap64;
416 BrainProducts) placed according to the extended 10–20 system (Klem et al., 1999). Sixty
417 electrodes were used of the most central scalp positions. The EEG was sampled at 500Hz,
418 referenced at FCz and grounded at Iz. For artifact removal, a horizontal, bipolar
419 electrooculogram (EOG) was recorded using two of the remaining electrodes and placing
420 them on the skin approximately 1cm left from the left eye and right from the right eye at
421 the height of the pupils. One vertical electrooculogram was recorded using one of the
422 remaining electrodes centrally approx. 1cm beneath the left eye lid and another electrode
423 was fixated on the neck at the upper part of the left trapezius muscle (Musculus trapezius)
424 to record an electromyogram (EMG).

425 EEG Preprocessing

426 The data analysis was performed using the Fieldtrip toolbox for EEG/MEG-analysis
427 (Oostenveld et al., 2011, Donders Institute for Brain, Cognition and Behaviour, Radboud

University Nijmegen, the Netherlands. See http://www.ru.nl/neuroimaging/fieldtrip). EEG data were epoched and time-locked to the stimulus onset using the electrical trigger signaling the thermode to start the temperature rise of a given pain trial. Each epoch included a time range 3410ms before and 2505ms after trigger onset.

The data was detrended and baseline correction was applied over the whole time range of each trial. The data was band-pass filtered at 1-100Hz, Butterworth, 4th order. EEG epochs were then visually inspected and trials contaminated by artifacts due to gross movements or technical artifacts were removed. Subsequently, trials contaminated by eye-blinks and movements were corrected using an independent component analysis (ICA) algorithm (Makeig et al., 1996; Jung et al., 2000). In all datasets, individual eye movements, showing a large EOG channel contribution and a frontal scalp distribution, were clearly seen in the removed independent components. Back-projection of the remaining non-artifactual components resulted in corrected data. Subsequently, the data was re-referenced to a common average of all EEG channels.

Before time-frequency transformations were performed, the time axis of single trials were shifted to create cue-locked and pain-locked data. Cue-locked data uses the onset of the triangular cue as t = 0. Pain-locked data takes the ramp up period of the thermode into account and sets t = 0 to the time point when the thermode reached the target temperature (225ms, 325ms and 375 after trigger onset for low, medium and high pain conditions, respectively). Frequencies up to 30 Hz were analyzed using a sliding Hanning-window Fourier transformation with a window length of 300ms and a step-size of 50ms. For the analysis of frequencies higher than 30Hz spectral analyses of the EEG data were performed using a sliding window multi-taper analysis. A window of 200ms length was shifted over the data with a step size of 50ms with a spectral smoothing of 15 Hz. Single trial z-normalization over the whole trial duration was performed (Grandchamp and Delorme, 2011) and afterwards, a z-baseline was calculated with a window of 500ms before cue onset (i.e. cue locked: -650ms to -150ms; pain locked: -2800ms to -2300ms for low pain, -2900ms to -2400ms for medium pain and -2950ms to -2450ms for high pain). For the purpose of source reconstruction, time-frequency windows were defined based on identified clusters in each frequency band. A Fast Fourier Transformation (FFT) of these regions was estimated with a Hanning taper with a full window of the significant time-frequency range of the respective cluster. Additionally, a time frame of 500ms before

cue onset (i.e. cue locked: -650ms to -150ms; pain locked: -2000ms to -2100ms) was chosen and the same source reconstruction procedure was performed and was subtracted from the cluster source representation as a stimulus baseline.

Source Reconstruction

For source reconstruction of expectation and prediction error effects, the 305-MNI Average Brain (Evans et al., 1993) was used with a triangulated mesh (consisting of 4000 / 2000 / 1000 triangles for brain, skull and scalp, respectively) to generate a realistic three-shell head model using fieldtrip. The head model was created using the fieldtrip implementation of the boundary element methods by Phillips et al. (2007). Standard electrode positions of the 10-20 system (Klem et al., 1999) were derived from a fieldtrip template and EEG electrodes were projected onto the scalp, while EOG and EMG electrodes were excluded from analysis.

Conductivity values were assigned to these three layers according to the conductivities reported by Oostendorp et al. (2000) who found a brain:skull:scalp ratio of 1:1/15:1. With the head model, mesh and electrode positions, a lead field matrix was estimated with a resolution of 5mm. For each effect of interest, all combinations of conditions were appended to calculate a cross-spectral density matrix to create a common spatial filter by means of the Fieldtrip implementation of the exact Low Resolution Electric Tomography (eLORETA) method (Pascual-Marqui et al., 2011). The common filter was then applied at each condition separately for source analysis using eLORETA. Statistical analysis performed at the electrode level were replicated in source space for display purposes and interpolated to a 256x256x256 voxel space to identify potential neuronal generators.

Predictive Coding Model

Similar to a previous fMRI study (Fazeli and Buechel, 2018), our full model was comprised of three experimental within-subject factors (see Fig. 2). The stimulus intensity factor (INT) models the measured response with a simple linear function of the stimulus intensity. The expectation (EXP) factor was defined (see Fig. 2; center column) linearly from the intensity predicted by the cue. Again, conditions with a low pain cue were coded with a -1, conditions with a medium pain cue with a 0 and conditions with a high pain cue with a 1. The absolute prediction error factor (PE) resulted from the absolute difference of the expectation and actual stimulus intensity (see Fig. 2; right column).

Behavioral Pain Ratings

Behavioral pain ratings were averaged for all 3x3 cue-stimulus combinations over each participant, resulting in a 35x9 matrix (subject x condition). We tested for main effects across stimulus intensity, expectation, as well as prediction error using rmANOVA as implemented in MATLAB (version 2016b, The MathWorks).

EEG data analysis

All statistical tests in electrode space were corrected for multiple comparisons using non-parametrical permutation tests of clusters (Maris & Oostenveld, 2007). Cluster permutation tests take into account that biological processes are not strictly locked to a single frequency or time point and that activity could be picked up by multiple electrodes. Cluster permutation tests are specifically useful for explorative testing, as explained by Maris & Oostenveld (2007). While prior hypotheses could have been formulated regarding the spatial, temporal and spectral characteristics of brain responses associated with the intensity of thermal stimulation and regions-of-interest could have been described, variations in the present design could be related to temporal and spectral differences compared to other studies which would be taken into account using non-parametric cluster permutation testing.

We wanted to explore positive and negative time-frequency patterns associated with our variations of stimulus intensity, expectation and absolute prediction errors using a repeated measures ANOVA. A statistical value corresponding to a p-value of .05 ($F(2,28) = 4.196$) obtained from the repeated measures ANOVA F-statistics of the respective main effect was used for clustering. Further, clustering was restricted in a way that only samples were included in a cluster which had at least one significant neighbor in electrode space, i.e. at least one neighboring channel also had to exceed the threshold for a sample to be included in the cluster).

Subsequently, a cluster value was defined as the sum of all statistical values of included samples. Monte Carlo sampling was used to generate 1000 random permutations of the design matrix and statistical tests were repeated in time-frequency space with the random design matrix. The probability of a cluster from the original design matrix (p-value) was calculated by the proportion of random design matrices producing a cluster with a cluster value exceeding the original cluster. This test was applied two-sided for

negative and positive clusters, which were differentiated by the average slope of the estimated factors. The cluster permutation test was done in a time frame from 0 to 1.6s from pain onset in order to restrict the analysis to the pain duration in spite of the shift in the time axis accounting for the ramp-up time of the thermode.

Acknowledgements

We would like to thank Markus Ploner for comments on an earlier version of this manuscript. C.B is supported by the DFG, SFB 289, M.R. is supported by the DFG SFB TR 169 project B3.

References

Albu S, Meagher MW (2016) Expectation of nocebo hyperalgesia affects EEG alpha-activity. Int J Psychophysiol 109:147–152.

Anchisi D, Zanon M (2015) A Bayesian perspective on sensory and cognitive integration in pain perception and placebo analgesia. PLoS ONE 10:e0117270.

Arnal LH, Giraud A-L (2012) Cortical oscillations and sensory predictions. Trends Cogn Sci (Regul Ed) 16:390–398.

Atlas LY, Bolger N, Lindquist MA, Wager TD (2010) Brain Mediators of Predictive Cue Effects on Perceived Pain. Journal of Neuroscience 30:12964–12977.

Atlas LY, Wager TD (2012) How expectations shape pain. Neurosci Lett 520:140–148.

Babiloni C, Brancucci A, Babiloni F, Capotosto P, Carducci F, Cincotti F, Arendt-Nielsen L, Chen ACN, Rossini PM (2003) Anticipatory cortical responses during the expectancy of a predictable painful stimulation. A high-resolution electroencephalography study. Eur J Neurosci 18:1692–1700.

Bastos AM, Usrey WM, Adams RA, Mangun GR, Fries P, Friston KJ (2012) Canonical microcircuits for predictive coding. Neuron 76:695–711.

Bingel U, Lorenz J, Schoell E, Weiller C, Büchel C (2006) Mechanisms of placebo analgesia: rACC recruitment of a subcortical antinociceptive network. Pain 120:8–15.

Büchel C, Geuter S, Sprenger C, Eippert F (2014) Placebo Analgesia: A Predictive Coding Perspective. Neuron 81:1223–1239.

Clark A (2013) Whatever next? Predictive brains, situated agents, and the future of cognitive science. Behav Brain Sci 36:181–204.

Colloca L, Benedetti F (2005) Placebos and painkillers: is mind as real as matter? Nat Rev Neurosci 6:545–552.

Ernst MO, Banks MS (2002) Humans integrate visual and haptic information in a statistically optimal fashion. Nature 415:429–433.

Fazeli S, Büchel C (2018) Pain-Related Expectation and Prediction Error Signals in the Anterior Insula Are Not Related to Aversiveness. J Neurosci 38:6461–6474.

Franciotti R, Ciancetta L, Della Penna S, Belardinelli P, Pizzella V, Romani GL (2009) Modulation of alpha oscillations in insular cortex reflects the threat of painful stimuli. Neuroimage 46:1082–1090.

Friston K (2010) The free-energy principle: a unified brain theory? Nat Rev Neurosci 11:127–138.

Geuter S, Boll S, Eippert F, Büchel C (2017) Functional dissociation of stimulus intensity encoding and predictive coding of pain in the insula. Elife 6.

566 Grahl A, Onat S, Büchel C (2018) The periaqueductal gray and Bayesian integration in
567 placebo analgesia. Elife 7.

568 Grandchamp R, Delorme A (2011) Single-Trial Normalization for Event-Related Spectral
569 Decomposition Reduces Sensitivity to Noisy Trials. Front Psychol 2 Available at:
570 https://www.ncbi.nlm.nih.gov/pmc/articles/PMC3183439/ [Accessed August
571 12, 2020].

572 Huang Y, Rao RPN (2011) Predictive coding. Wiley Interdisciplinary Reviews-Cognitive
573 Science 2:580–593.

574 Huneke NTM, Brown CA, Burford E, Watson A, Trujillo-Barreto NJ, El-Deredy W, Jones
575 AKP (2013) Experimental placebo analgesia changes resting-state alpha
576 oscillations. PLoS ONE 8:e78278.

577 Jung TP, Makeig S, Humphries C, Lee TW, McKeown MJ, Iragui V, Sejnowski TJ (2000)
578 Removing electroencephalographic artifacts by blind source separation.
579 Psychophysiology 37:163–178.

580 Knill DC, Pouget A (2004) The Bayesian brain: the role of uncertainty in neural coding and
581 computation. Trends Neurosci 27:712–719.

582 Koyama T, McHaffie JG, Laurienti PJ, Coghill RC (2005) The subjective experience of pain:
583 where expectations become reality. Proc Natl Acad Sci USA 102:12950–12955.

584 Lorenz J, Garcia-Larrea L (2003) Contribution of attentional and cognitive factors to laser
585 evoked brain potentials. Neurophysiol Clin 33:293–301.

586 Makeig S, Bell A, Jung T-P, Sejnowski T (1996) Independent Component Analysis of
587 Electroencephalographic Data. 8.

588 Mitra PP, Pesaran B (1999) Analysis of Dynamic Brain Imaging Data. Biophysical Journal
589 76:691–708.

590 Nickel MM, Dinh ST, May ES, Tiemann L, Hohn VD, Gross J, Ploner M (2020) Neural
591 oscillations and connectivity characterizing the state of tonic experimental pain in
592 humans. Human Brain Mapping 41:17–29.

593 Ongaro G, Kaptchuk TJ (2019) Symptom perception, placebo effects, and the Bayesian
594 brain. Pain 160:1–4.

595 Pascual-Marqui RD, Michel CM, Lehmann D (1994) Low resolution electromagnetic
596 tomography: a new method for localizing electrical activity in the brain. Int J
597 Psychophysiol 18:49–65.

598 Petrovic P, Kalso E, Petersson KM, Ingvar M (2002) Placebo and opioid analgesia--
599 imaging a shared neuronal network. Science 295:1737–1740.

600 Ploghaus A, Tracey I, Gati JS, Clare S, Menon RS, Matthews PM, Rawlins JN (1999)
601 Dissociating pain from its anticipation in the human brain. Science 284:1979–
602 1981.

603 Ploner M, Gross J, Timmermann L, Pollok B, Schnitzler A (2006) Pain suppresses
604 spontaneous brain rhythms. Cereb Cortex 16:537–540.

605 Ploner M, Sorg C, Gross J (2017) Brain Rhythms of Pain. Trends Cogn Sci (Regul Ed)
606 21:100–110.

607 Song Y, Yao M, Kemprecos H, Byrne Á, Xiao Z, Zhang Q, Singh A, Wang J, Chen ZS (2019)
608 Predictive Coding Models for Pain Perception. Neuroscience. Available at:
609 http://biorxiv.org/lookup/doi/10.1101/843284 [Accessed March 31, 2020].

610 Tiemann L, May ES, Postorino M, Schulz E, Nickel MM, Bingel U, Ploner M (2015)
611 Differential neurophysiological correlates of bottom-up and top-down
612 modulations of pain. Pain 156:289–296.

613 Todorovic A, van Ede F, Maris E, de lange FP (2011) Prior Expectation Mediates Neural
614 Adaptation to Repeated Sounds in the Auditory Cortex: An MEG Study. Journal of
615 Neuroscience 31:9118–9123.

616 Tracey I, Mantyh PW (2007) The cerebral signature for pain perception and its
617 modulation. Neuron 55:377–391.

618 van Pelt S, Heil L, Kwisthout J, Ondobaka S, van Rooij I, Bekkering H (2016) Beta- and
619 gamma-band activity reflect predictive coding in the processing of causal events.
620 Soc Cogn Affect Neurosci 11:973–980.

621 Wager TD, Rilling JK, Smith EE, Sokolik A, Casey KL, Davidson RJ, Kosslyn SM, Rose RM,
622 Cohen JD (2004) Placebo-induced changes in FMRI in the anticipation and
623 experience of pain. Science 303:1162–1167.

624 Wiech K (2016) Deconstructing the sensation of pain: The influence of cognitive processes
625 on pain perception. Science 354:584–587.

626 Wiech K, Ploner M, Tracey I (2008) Neurocognitive aspects of pain perception. Trends
627 Cogn Sci (Regul Ed) 12:306–313.

628 Xiao Z, Martinez E, Kulkarni PM, Zhang Q, Hou Q, Rosenberg D, Talay R, Shalot L, Zhou H,
629 Wang J, Chen ZS (2019) Cortical Pain Processing in the Rat Anterior Cingulate
630 Cortex and Primary Somatosensory Cortex. Front Cell Neurosci 13:165.

631 Zhang ZG, Hu L, Hung YS, Mouraux A, Iannetti GD (2012) Gamma-band oscillations in the
632 primary somatosensory cortex--a direct and obligatory correlate of subjective pain
633 intensity. J Neurosci 32:7429–7438.

Supplementary Materials

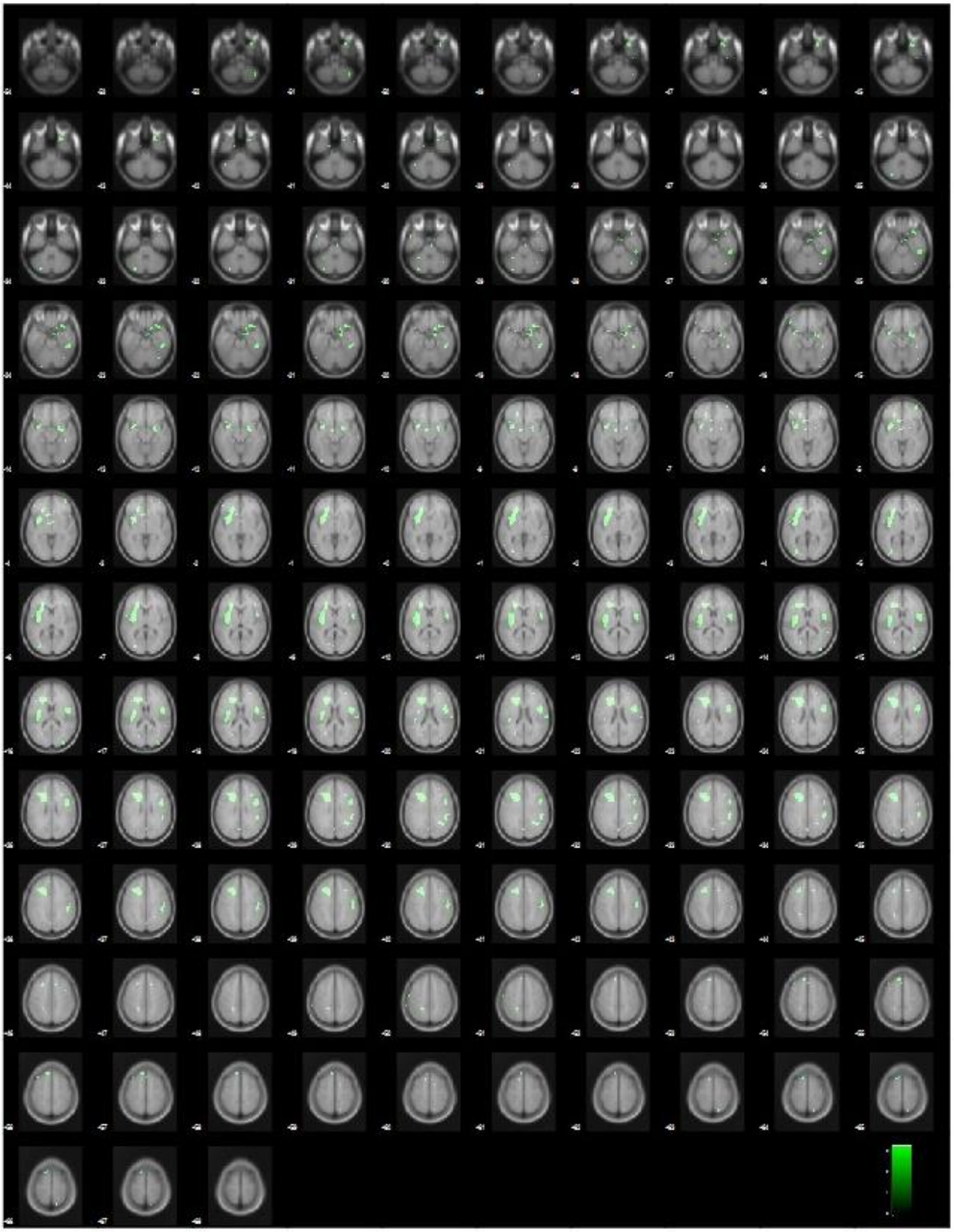

Supplemental Figure 1. The distribution of the reconstructed expectation (EXP) cluster in axial slices (1mm gap), representing the top 2.5% statistical values in source space overlaid on a structural MR template.

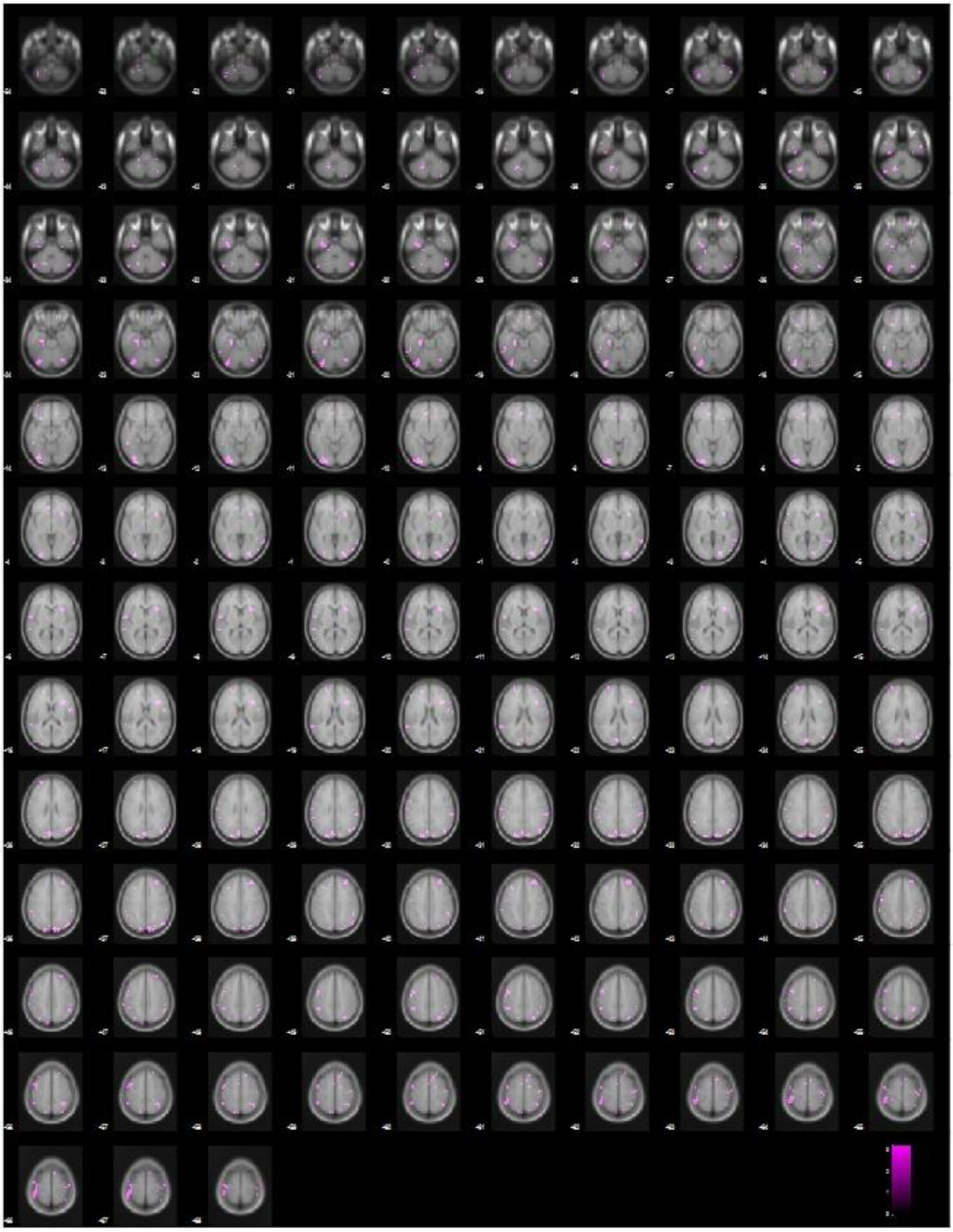

Supplemental Figure 2. The distribution of the reconstructed absolute prediction error (PE) cluster in axial slices (1mm gap), representing the top 2.5% statistical values in source space overlaid on a structural MR template.